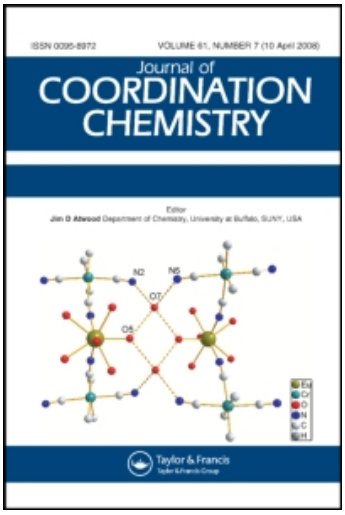

Journal of Coordination Chemistry
Publication details, including instructions for authors and subscription information:
http://www.informaworld.com/smpp/title~content=t713455674

Synthesis, characterization, DNA binding, oxidative damage of DNA strand scission, and antimicrobial activities of β-diketone condensed Schiff-base transition metal complexes

N. Raman[a]; R. Jeyamurugan[a]; R. Usha Rani[a]; T. Baskaran[a]; L. Mitu[b]
[a] Research Department of Chemistry, VHNSN College, Virudhunagar 626001, Tamil Nadu, India [b] Department of Physics and Chemistry, University of Pitesti, Pitesti 110040, Romania

First published on: 18 May 2010

To cite this Article Raman, N. , Jeyamurugan, R. , Rani, R. Usha , Baskaran, T. and Mitu, L.(2010) 'Synthesis, characterization, DNA binding, oxidative damage of DNA strand scission, and antimicrobial activities of β-diketone condensed Schiff-base transition metal complexes', Journal of Coordination Chemistry, 63: 9, 1629 — 1644, First published on: 18 May 2010 (iFirst)
To link to this Article: DOI: 10.1080/00958972.2010.485643
URL: http://dx.doi.org/10.1080/00958972.2010.485643

Journal of Coordination Chemistry
Vol. 63, No. 9, 10 May 2010, 1629–1644

Taylor & Francis
Taylor & Francis Group

Synthesis, characterization, DNA binding, oxidative damage of DNA strand scission, and antimicrobial activities of β-diketone condensed Schiff-base transition metal complexes

N. RAMAN*†, R. JEYAMURUGAN†, R. USHA RANI†,
T. BASKARAN† and L. MITU‡

†Research Department of Chemistry, VHNSN College,
Virudhunagar 626001, Tamil Nadu, India
‡Department of Physics and Chemistry, University of Pitesti,
Pitesti 110040, Romania

(*Received 20 November 2009; in final form 3 February 2010*)

Co(II), Ni(II), Cu(II), Zn(II), and VO(IV) complexes containing a versatile β-diketone Schiff-base ligand (obtained by the condensation of 3-furan-2-ylmethylene-2,4-dione and 2-aminophenol) have been synthesized and characterized. Microanalytical, magnetic, and spectroscopic data reveal that the central metal is coordinated to two oxygens of phenolate and two nitrogens of imine of the ligand. Binding of synthesized complexes with calf thymus DNA has been investigated by spectroscopic and electrochemical methods and viscosity measurements. The complexes are able to form adducts with DNA and to distort the double helix by changing the base stacking. Electrostatic binding of vanadyl complex is observed from the weak hypochromism in electronic absorption spectra and no change in the viscosity with DNA. Oxidative DNA cleavage activities of the complexes are studied with supercoiled pUC19 DNA using gel electrophoresis. The hydroxyl radical ($OH^{\bullet}$) is likely to be the species responsible for the cleavage of pUC19 DNA by the synthesized complexes. Under our experimental conditions, the vanadyl complex has no significant cleavage of DNA. The compounds have been screened for activity against several bacterial and fungal strains and the results are compared with the activity of standard drugs.

Keywords: DNA binding; DNA cleavage; Complexes; Schiff base; Antimicrobial

1. Introduction

The interaction of transition metal compounds with DNA has been extensively studied. Due to the unusual binding properties and general photoactivity, these coordination compounds were suitable candidates as DNA secondary structure probes, photocleavers, and antitumor drugs [1–3]. Transition metal complexes can bind to DNA by non-covalent interactions such as external surface binding for cations, groove binding for large molecules, and intercalating system. Among the factors governing the binding modes, it appears that the most significant is the molecular shape. Those complexes that best fit against the DNA helical structure display the highest binding affinity [4, 5].

*Corresponding author. Email: drn_raman@yahoo.co.in

Journal of Coordination Chemistry
ISSN 0095-8972 print/ISSN 1029-0389 online
DOI: 10.1080/00958972.2010.485643

Applications of these complexes require that the complex bind to DNA through an intercalative mode with the ligand intercalating into the adjacent base pairs of DNA. In fact, some of these complexes also exhibit interesting properties upon binding to DNA [6–8].

In this article, we synthesized Co(II), Ni(II), Cu(II), Zn(II), and VO(IV) complexes containing a β-diketone ligand with phenolic oxygen and azomethine nitrogen and studied their binding properties to calf thymus DNA (CT DNA) using absorption spectroscopy, cyclic DPV (differential pulse voltammogram), and viscosity measurements. Their oxidative cleavage behavior toward pUC19 DNA and the mechanism for cleavage were also investigated. The result should be of value in understanding the binding of complex to DNA as well as laying the foundation for the design of DNA molecular light switch and DNA cleaving agents [9].

2. Experimental

2.1. *Chemicals*

All reagents were procured from Merck. The solvents used for electrochemical and spectroscopic studies were purified by standard procedures [10]. Supercoiled (SC) pUC19 (cesium chloride purified) DNA was purchased from Bangalore Genei (India). DNA solution in 5 mmol Tris–HCl/50 mmol NaCl (pH 7.2) buffer medium gave a ratio of UV absorbance at 260–280 nm of *ca* 1.8–1.9, indicating that the DNA was sufficiently free from protein [11]. The DNA concentration per nucleotide was determined by absorption spectroscopy using the molar absorption coefficient ($6600\,mol^{-1}\,cm^{-1}$) at 260 nm [12]. Stock solutions were stored at 4°C and used within 4 days. Agarose (molecular biology grade), ethidium bromide (EB), and tetrabutylammonium perchlorate were obtained from Sigma (USA). Tris–HCl buffer solution was prepared using deionized, sonicated triply-distilled water.

2.2. *Physical measurements*

Elemental analyses (C, H, N, and S) were carried out with a Carlo Erba 1108 analyzer. Infrared (IR) spectra of the samples were recorded in the region 4000–400 cm^{-1} using KBr pellets and a Perkin Elmer 783 spectrophotometer. Proton nuclear magnetic resonance (^{1}H-NMR) spectra (300 MHz) of the samples were recorded in $CDCl_3$ and DMSO-d_6 with TMS as internal standard on a Bruker Avance DRX 300 FT-NMR (FT, Fourier transform) spectrometer. Fast atom bombardment mass spectra (FAB-MS) were obtained using a VGZAB-HS spectrometer in a 3-nitrobenzyl alcohol matrix. The X-band electron spin resonance (ESR) spectra of the complexes were recorded at 300 and 77 K using tetracyanoethylene (TCNE) as the g-marker. Electronic absorption spectra were recorded using a Shimadzu UV-1601 spectrophotometer. Magnetic susceptibility measurements of the complexes were carried out by Gouy balance using copper sulfate as the calibrant. The purity of the ligand and its complexes was evaluated by column chromatography and thin layer chromatography. Antimicrobial activity was carried out in the Research Department of Chemistry,

VHNSN College, Virudhunagar, in association with the Department of Microbiology of the same institute.

2.3. *Preparation of Schiff-base ligand*

The non-enolizable diketone was prepared by using the modified procedure reported earlier [13]. Acetylacetone (10 mmol) was mixed with furfuraldehyde (10 mmol) and piperidine, and the reaction mixture was stirred thoroughly for *ca* 5 h with occasional cooling. Gradually, a dark brown precipitate separated in small amounts. The reaction mixture was set aside to evaporate to dryness and the residual solid was washed with an excess of petroleum ether to remove the unreacted reagents. The obtained solid product was recrystallized from $CHCl_3$–petroleum ether to give a pure brown Knoevenagel condensate (3-furan-2-ylmethylene-2,4-dione) that was used as the starting material for the preparation of Schiff base.

3-Furan-2-ylmethylene-2,4-dione (10 mmol) in 50 mL of ethanol was refluxed with 2-aminophenol (20 mmol) for 6 h after the addition of potassium carbonate. The potassium carbonate was filtered off from the reaction mixture and the solvent was evaporated to dryness. The residual solid was washed with an excess of petroleum ether to remove any unreacted reagents and the dark brown powder was filtered and dried *in vacuo*. Yield: 68%. IR (KBr): 3100–3000, (–OH); 1634, (–C=N); 2928, (–C–CH_3) cm^{-1}. ^{1}H-NMR ($CDCl_3$): δ(–OH), 10.1 (s); (phenyl multiplet), 6.6–7.2 δ(m); δ(–CH_3), 2.0 (s); δ(–CH=C–), 5.8 (s). MS *m*/*z*: 361, (M + 1); 145, $[C_9H_9N_2]^+$; 93, $[C_6H_5O]^+$; 77, $[C_6H_5]^+$; 68, $[C_4H_4O]^+$; 41, $[CH_3CN]^+$. Anal. Calcd for $C_{22}H_{20}N_2O_3$ (%): C, 73.3; H, 5.6; N, 7.7; Found (%): C, 73.1; H, 5.6; N, 7.6. λ_{max} (EtOH, cm^{-1}): 34,482, 30,864. The outline of the synthesis of ligand is shown in scheme 1.

2.4. *Synthesis of metal complexes*

A solution of the metal chloride (5 mmol) in absolute ethanol (20 mL) was added to a solution of the ligand (5 mmol) in absolute ethanol (25 mL) and the mixture was refluxed for 3–4 h. The end of the reaction was determined by thin-layer chromatography; the precipitate was filtered off, washed with ethanol and diethyl ether, and dried *in vacuo*.

[$CoL(H_2O)_2$]: Yield: 49%. IR (KBr, cm^{-1}): 3432, (–OH of H_2O), 2922 (–C–CH_3), 1600 (C=N), 450 (M–N), and 480 (M–O). MS *m*/*z*: 454, (M + 1); 418, $[CoL]^+$; 358, $[C_{22}H_{18}N_2O_3]^+$; 145, $[C_9H_9N_2]^+$; 93, $[C_6H_5O]^+$; 77, $[C_6H_5]^+$; 68, $[C_4H_4O]^+$; 41, $[CH_3CN]^+$. Anal. Calcd for [$CoC_{22}H_{22}N_2O_5$] (%): Co, 13.0; C, 58.3; H, 4.9; N, 6.2; Found (%): Co, 12.8; C, 58.0; H, 4.8; and N, 6.0. Λ_M ($Ohm^{-1}\,cm^2\,mol^{-1}$), 1.6×10^{-3}; μ_{eff} (B.M.), 3.75. λ_{max} (DMF, cm^{-1}): 37,652; 29,239; 15,408.

[NiL]: Yield: 43%. IR (KBr, cm^{-1}): 2925, (–C–CH_3); 1603, (C=N); 452, (M–N); 476, (M–O). MS *m*/*z*: 417, (M^+); 358, $[C_{22}H_{18}N_2O_3]^+$; 145, $[C_9H_9N_2]^+$; 93, $[C_6H_5O]^+$; 77, $[C_6H_5]^+$; 68, $[C_4H_4O]^+$; 41, $[CH_3CN]^+$. ^{1}H-NMR (DMSO-d_6): (phenyl multiplet), 6.8–7.1 δ(m); δ(CH_3), 2.3 (s); δ(–CH=C–), 5.4 (s). Anal. Calcd for [$NiC_{22}H_{18}N_2O_3$] (%): Ni, 14.1; C, 63.4; H, 4.4; N, 6.7; Found (%): Ni, 13.8; C, 63.1; H, 4.3; N, 6.6. Λ_M ($Ohm^{-1}\,cm^2\,mol^{-1}$), 1.8×10^{-3}; μ_{eff} (B.M.), diamagnetic. λ_{max} (DMF, cm^{-1}): 23,256; 36,214; 14,184; 19,417.

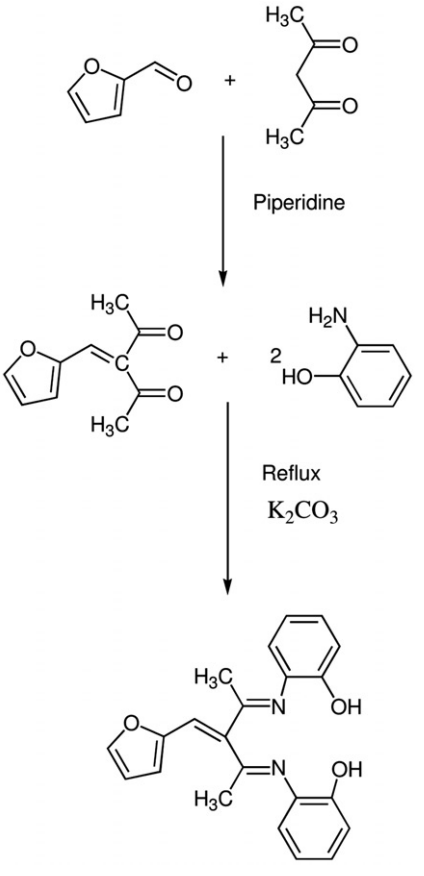

Scheme 1. Outline of the synthesis of ligand.

[CuL]: Yield: 54%. IR (KBr, cm^{-1}): 2930, (–C–CH_3); 1598, (C=N); 446, (M–N); 482, (M–O). MS *m/z*: 422, (M^+); 424, (M + 2); 358, $[C_{22}H_{18}N_2O_3]^+$; 145, $[C_9H_9N_2]^+$; 93, $[C_6H_5O]^+$; 77, $[C_6H_5]^+$; 68, $[C_4H_4O]^+$; 41, $[CH_3CN]^+$. Anal. Calcd for $[CuC_{22}H_{18}N_2O_3]$ (%): Cu, 15.1; C, 62.6; H, 4.3; N, 6.6; Found (%): Cu, 14.9; C, 62.3; H, 4.3; N, 6.5. Λ_M ($Ohm^{-1}\,cm^2\,mol^{-1}$), 3.3×10^{-3}; μ_{eff} (B.M.), 1.8. λ_{max} (DMF, $mol^{-1}\,cm^{-1}$): 22,988; 35,714; 16,391.

[ZnL]: Yield: 38%. IR (KBr, cm^{-1}): 2924, (–C–CH_3); 1593, (C=N); 453, (M–N); 470, (M–O). MS *m/z*: 424, (M^+); 358, $[C_{22}H_{18}N_2O_3]^+$; 145, $[C_9H_9N_2]^+$; 93, $[C_6H_5O]^+$; 77, $[C_6H_5]^+$; 68, $[C_4H_4O]^+$; 41, $[CH_3CN]^+$. ^{1}H-NMR (DMSO-d_6): (phenyl multiplet), 6.5–7.0 δ(m); $\delta(CH_3)$, 2.1 (s); δ(–CH=C–), 5.6 (s). Anal. Calcd for $[ZnC_{22}H_{18}N_2O_3]$ (%): Zn, 15.4; C, 62.4; H, 4.3; N, 6.6; Found (%): Zn, 15.0; C, 62.1; H, 4.3; N, 6.6. Λ_M ($Ohm^{-1}\,cm^2\,mol^{-1}$), 0.8×10^{-3}; μ_{eff} (B.M.), diamagnetic. λ_{max} (DMF, cm^{-1}): 21,259; 33,658.

[VOL]: Yield: 40%. IR (KBr): 2924, (–C–CH_3); 1596, (C=N); 450, (M–N); 478, (M–O). MS *m/z*: 426, (M + 1); 360, $[C_{22}H_{18}N_2O_3]^+$; 41, $[CH_3CN]^+$; 68, $[C_4H_4O]^+$; 77, $[C_6H_5]^+$; 93, $[C_6H_5O]^+$; 109, $[C_9H_9N_2]^+$. Anal. Calcd for $[VC_{22}H_{18}N_2O_4]$ (%): V, 12.0; C, 62.1; H, 4.3; N, 6.6; Found (%): V, 11.8; C, 61.8; H, 4.2; N, 6.4%.

Λ_M ($Ohm^{-1}\,cm^2\,mol^{-1}$), 2×10^{-3}; μ_{eff} (B.M.), 1.79. λ_{max} (DMF, cm^{-1}): 22,547; 36,982; 12,165; 19,157.

2.5. *DNA binding and cleavage experiments*

Electronic absorption spectra were measured on a Shimadzu UV-1601 spectrophotometer in 5 mmol L^{-1} Tris–HCl buffer (pH 7.1) containing 50 mmol L^{-1} NaCl at room temperature. Synthesized complexes were dissolved in DMF at 2.5×10^{-3} mol L^{-1}. Working solutions were prepared by the dilution of the synthesized complexes in 5 mmol L^{-1} Tris–HCl buffer to 25 μmol L^{-1}.

Absorption titration experiments were performed by maintaining the metal complex concentration at 25 μmol L^{-1}, while varying the concentration of the CT DNA from 0 to 400 μmol L^{-1}. While measuring the absorption spectra, equal quantity of CT DNA was added to both the complex solution and the reference solution to eliminate the absorbance of CT DNA itself. From the absorption data, the intrinsic binding constant K_b was determined from a plot of [DNA]/($\varepsilon_a - \varepsilon_f$) *versus* [DNA] using equation (1):

$$[DNA]/(\varepsilon_a - \varepsilon_f) = [DNA]/(\varepsilon_b - \varepsilon_f) + [K_b(\varepsilon_b - \varepsilon_f)]^{-1} \quad (1)$$

where [DNA] is the concentration of CT DNA in base pairs. The apparent absorption coefficients ε_a, ε_f, and ε_b correspond to A_{obsd}/[M], the extinction coefficient for the free metal(II) complex, and extinction coefficient for the metal(II) complex in the fully bound form, respectively [14]. K_b is given by the ratio of slope to intercept.

Cyclic voltammetric and DPV studies were performed on a CHI 620C electrochemical analyzer with a three electrode system of glassy carbon (GC) as the working electrode, a platinum wire as auxiliary electrode, and Ag/AgCl as the reference electrode. All the voltammetric experiments were carried out in single-compartment cells of 5–15 mL. Solutions were deoxygenated by purging with N_2 prior to measurements. Increasing amounts of CT DNA were added directly into the cell containing the solution (2.5×10^{-3} mol L^{-1}, 5 mmol L^{-1} Tris–HCl/50 mmol L^{-1} NaCl buffer, pH 7.1). The concentration ranged from 0 to 400 μmol L^{-1} for CT DNA. The solution in the cuvette was thoroughly mixed before each scan. All the experiments were carried out at room temperature.

Viscosity experiments were carried on an Ostwald viscometer immersed in a thermostated water bath maintained at 30.0 ± 0.1°C. DNA samples of approximately 0.5 mmol L^{-1} were prepared by sonicating in order minimize the complexities arising from DNA flexibility [15]. Flow time was measured with a digital stopwatch three times for each sample and an average flow time was calculated. Data are presented as $(\eta/\eta^0)^{1/3}$ *versus* the concentration of the complex, where η is the viscosity of DNA solution in the presence of complex and η^0 is the viscosity of DNA solution in the absence of complex. Viscosity values were calculated after correcting the flow time of buffer alone (t_0), $\eta = (t - t_0)/t_0$ [16].

The extent of cleavage of SC pUC19 DNA (33.3 μmol L^{-1}, 0.2 μg) to its nicked circular (NC) form was determined by agarose gel electrophoresis in 50 mmol L^{-1} Tris–HCl buffer (pH 7.2) containing 50 mmol L^{-1} NaCl. The gel electrophoresis experiments were performed by incubation of 30 μmol L^{-1} of pUC19 DNA, 50 μmol L^{-1} of complex, and 50 μmol L^{-1} 3-mercaptopropionic acid (MPA) in Tris–HCl buffer (pH 7.2) at 37°C for 2 h. After incubation, the samples were electrophoresed for 2 h

at 100 V on 0.8% agarose gel using Tris–acetic acid–EDTA buffer (pH 7.2). The gel was then stained using 1 μg cm^{-3} EB and photographed under ultraviolet light at 360 nm. All the experiments were performed at room temperature unless otherwise mentioned.

2.6. *Antimicrobial assays*

The ligand and its complexes were tested for their *in vitro* antimicrobial activity against Gram-positive bacteria *Staphylococcus aureus* and *Bacillus subtilis*, Gram-negative bacteria *Escherichia coli* and *Salmonella typhi* by the disk diffusion method using agar nutrient as the medium and fungi *Aspergillus niger*, *Aspergillus flavus*, *Candida albicans*, and *Rhizoctonia bataicola* by disk diffusion method using potato dextrose agar as medium. The stock solution (10^{-2} mol L^{-1}) was prepared by dissolving the compounds in DMSO and the solutions were serially diluted in order to find the minimum inhibitory concentration (MIC) values. In a typical procedure [17], a disk was made on the agar medium inoculated with microorganisms. The disk was filled with the test solution using a micropipette and the plate was incubated, 24 h for bacteria and 72 h for fungi at 35°C. During this period, the test solution diffused and the growth of the inoculated microorganisms was affected. The inhibition zone was developed, at which the concentration was noted. Streptomysin and nystatin were used as control drugs.

3. Results and discussion

The Schiff base and its Cu(II), Co(II), Ni(II), VO(IV), and Zn(II) complexes are air stable. The ligand is soluble in chloroform, DMF, and DMSO, but the complexes are soluble only in DMF and DMSO. The ligand and complexes have been characterized by microanalytical, magnetic susceptibility, molar conductance, FAB-mass, IR, UV-Vis, ^{1}H-NMR, and electron paramagnetic resonance (EPR) spectral studies.

3.1. *Elemental analysis and molar conductance*

Elemental analyses for the metal complexes agree with the calculated values showing that the complexes have 1 : 1 metal : ligand ratio. The observed low molar conductances in DMF (10^{-3} mol L^{-1}) at room temperature are consistent with non-electrolytes. The absence of chloride is evident from Volhard's test and sulfate ion by $BaCl_2$ test.

3.2. *Mass spectra*

The FAB-MS of the ligand and its complexes were recorded and compared. The mass spectrum of the ligand shows (M + 1) peak at *m*/*z* 361 corresponding to $[C_{22}H_{20}N_2O_3]^+$. Also, the spectrum exhibited fragments at *m*/*z* 41, 68, 77, 93, and 145 corresponding to $[CH_3CN]^+$, $[C_4H_4O]^+$, $[C_6H_5]^+$, $[C_6H_5O]^+$, and $[C_9H_9N_2]^+$, respectively. The mass spectrum of $[CuC_{22}H_{20}N_2O_3]$ shows peaks at 422 and 424. The one at 422 may represent the molecular ion (M^+) peak of the complex and the other peak at 424 is an

isotopic fragment (M + 2). In all the complexes, the strongest peak (base beak) obtained at m/z 358 represents the stable species $[C_{22}H_{18}N_2O_3]^+$. Further, the spectra exhibited fragments at m/z 41, 68, 77, 93, and 145 corresponding to $[CH_3CN]^+$, $[C_4H_4O]^+$, $[C_6H_5]^+$, $[C_6H_5O]^+$, and $[C_9H_9N_2]^+$, respectively. The m/z of all the fragments of the ligand and its complexes confirm that the stoichiometry of the complexes is [ML] except cobalt complex, in which the mass spectrum shows two prominent peaks at 454 and 418. The peak at 454 may represent the molecular ion peak [M + 1], confirming the stoichiometry $[CoL(H_2O)_2]^+$ and the peak at 418 may indicate $[CoL]^+$. In all the complexes, the observed peaks are in good agreement with their empirical formula as indicated from the microanalytical data. Thus, the mass spectral data reinforce the conclusion drawn from the analytical and conductance values.

3.3. *IR spectra*

The ligand shows a broad band for the –OH group at *ca* 3100–3000 cm^{-1}. The disappearance of this peak in spectra of the complexes indicates the deprotonation of –OH on complexation. The spectrum of the ligand shows the characteristic –C=N bands at 1634 cm^{-1}, which shift to lower frequencies in spectra of all the complexes (1600 cm^{-1}), indicating azomethine nitrogen coordination to the metal [18]. Accordingly, the ligand is a tetradentate chelate, bonded to the metal *via* two nitrogens (–C=N) and two phenolic oxygens of the Schiff base. Assignment of the proposed coordination sites is further supported by medium bands at 450 and 480 cm^{-1}, attributed to ν_{M-N} and ν_{M-O}, respectively [19]. In addition to the other bands, the vanadyl complex shows a band at 960 cm^{-1} attributed to V=O frequency [20].

3.4. *Electronic absorption spectra*

The absorption spectrum of the ligand recorded in ethanol exhibits bands at 34,482 and 30,864 cm^{-1}, attributed to π–π^* and n–π^* transitions, respectively. The absorption spectrum of the copper(II) complex in DMF reveals characteristic bands of metal to ligand charge transfer (MLCT) transitions at 22,988 and 35,714 cm^{-1}. A strong absorption maximum at 16,391 cm^{-1} is assigned to d–d transition, characteristic of square-planar d^9 copper complex involving (d_{xz}, $d_{yz} \rightarrow d_{x^2-y^2}$) orbitals [21]. These transitions are usually made up of three spin-allowed transitions namely: $^2B_{1g} \rightarrow {}^2A_{1g}$, $^2B_{1g} \rightarrow {}^2B_{2g}$, and $^2B_{1g} \rightarrow {}^2E_g$. Two of these transitions are indicated by weaker shoulders in the absorption spectrum. The magnetic susceptibility in the solid state shows that the copper complex is paramagnetic with magnetic moment (1.8 B.M.) in the range normally found for square-planar copper complexes.

Square-planar complexes of nickel can readily be distinguished from octahedral or tetrahedral derivatives, in that no electronic transition occurs below 10,000 cm^{-1} [21], as a consequence of the large crystal field splitting in a square-planar complex. In the present complex, this band does not appear indicating square-planar geometry. The electronic absorption spectrum of cobalt complex gives only one d–d band at 15,408 cm^{-1} corresponding to $^4T_{1g} \rightarrow {}^4A_{2g}$ and other bands at 29,239 and 45,045 cm^{-1} which are characteristic of octahedral ligand field around Co(II) and can be assigned to $\pi \rightarrow \pi^*$ and $n \rightarrow \pi^*$ charge transfer transitions. The magnetic moment measurement indicates that the Co(II) complex is paramagnetic and the magnetic moment value is

nearer to the spin-only value for a high-spin octahedral complex. The magnetic moment values for high-spin Co(II) octahedral complexes fall in the range of 3.87–5.20 B.M. [21, 22].

Room temperature magnetic moment of the VO(IV) complex is 1.79 B.M., as that expected for oxovanadium(IV)-monomeric chelates with one unpaired electron. The electronic spectrum of oxovanadium complex exhibits bands at 12,165 and 19,157 cm^{-1} assigned to $^2B_2 \rightarrow {}^2E$ and $^2B_2 \rightarrow {}^2A_1$, respectively. The geometry of this five-coordinate mononuclear complex can be described as trigonal bipyramidal distorted toward a tetragonal pyramid or square pyramid [23].

3.5. *Nuclear magnetic resonance spectra*

The ^{1}H-NMR spectra of the ligand and its complexes (zinc and nickel) were recorded in $CDCl_3$ and DMSO-d_6, respectively. The ligand gives the following signals: (phenyl as multiplet) at 6.6–7.2 δ, –CH_3 at 2.0 δ, and –CH=C– at 5.8 δ. The peak at 10.1 δ is attributable to the phenolic –OH group present in 2-aminophenol. The absence of this peak for the complexes confirms the loss of the −OH proton in complexation. The azomethine proton signal in the spectra of the complexes shifts downfield compared to the free ligand, suggesting deshielding of the azomethine group due to coordination. There is no appreciable change in all of the other signals of the complexes.

3.6. *Electron spin resonance spectra*

The X-band ESR spectrum of [CuL] at 300 K shows an intense absorption at high field. However, this complex in frozen state shows four well-resolved peaks with low intensities in the low-field region and one intense peak in the high-field region. The magnetic susceptibility of 1.8 B.M. indicates that the complex is mononuclear. This is also evident from the absence of a half-field signal, observed in the spectrum at 1600 G due to the $m_s = \pm 2$ transitions, ruling out Cu–Cu interaction [23].

In square-planar complexes, the unpaired electron is in the $d_{x^2-y^2}$ orbital giving $^2B_{1g}$ as the ground state with $g_\parallel > g_\perp > 2$. From the observed values ($A_\parallel = 169 > A_\perp = 52$; $g_\parallel = 2.34 > g_\perp = 2.05 > 2$) it is clear that the ESR parameters coincide well with related square-planar systems [24]. In the axial spectrum, the g-values are related with exchange interaction coupling constant (G) by the expression, $G = g_\parallel - 2/g_\perp - 2$. According to Hathaway and Tomlinson [25], if the G value is larger than 4, exchange interaction is negligible. If the value of G is less than 4, the exchange interaction is considerable. For the present copper complex, the G value of 6.8 suggests that the local tetragonal axes are aligned parallel or slightly misaligned, consistent with a $d_{x^2-y^2}$ ground state.

The in-plane σ-bonding covalency parameter, α^2, is related to $A_\parallel$, $g_\parallel$, and $g_\perp$ according to the following equation [26]:

$$\alpha^2 = (A_\parallel / P) + (g_\parallel - 2.0023) + 3/7(g_\perp - 2.0023) + 0.04.$$

If the value of $\alpha^2 = 0.5$, it indicates complete covalent bonding, while the value of $\alpha^2 = 1.0$ suggests complete ionic bonding. The observed value of α^2 (0.56) indicates that the complex has some covalent character. The out-of-plane π-bonding

(γ^2) and in-plane π-bonding (β^2) parameters are calculated from the following expressions:

$$\beta^2 = (g_\parallel - 2.0023)E/(-8\lambda\alpha^2)$$
$$\gamma^2 = (g_\perp - 2.0023)E/(-2\lambda\alpha^2).$$

In these equations, $\lambda = -828\,\mathrm{cm}^{-1}$ for the free metal ion. The observed β^2 (1.72) and α^2 (0.56) values indicate that there is interaction in the out-of-plane π-bonding, whereas the in-plane π-bonding is completely ionic. This is also confirmed by the orbital reduction factors which are estimated using the following relations:

$$K_\parallel^2 = [(g_\parallel - 2.0023)\Delta E]/8\lambda_o$$
$$K_\perp^2 = [(g_\perp - 2.0023)\Delta E]/2\lambda_o,$$

where λ_o is the spin orbit coupling constant for the copper(II) ion ($-828\,\mathrm{cm}^{-1}$). $K_\parallel$ and $K_\perp$ are the parallel and perpendicular components of the orbital reduction factor (K), respectively. Significant information about the nature of bonding in the copper(II) complex can be derived from the relative magnitudes of $K_\parallel$ and $K_\perp$. In the case of pure σ-bonding $K_\parallel \approx K_\perp = 0.77$, whereas $K_\parallel < K_\perp$ implies considerable in-plane π-bonding while for out-of-plane π-bonding $K_\parallel > K_\perp$. For the present complex, the observed order is $K_\parallel$ (0.96) > $K_\perp$ (0.54) implying a greater contribution from out-of-plane π-bonding than from in-plane π-bonding.

EPR spectra of the vanadyl complex recorded in DMSO solution at 300 and 77 K show typical 8-line and 16-line patterns, respectively. The room temperature (300 K) spectrum shows that a single vanadium is present in the molecule, i.e., it is a monomer. In the frozen solid state, the spectrum shows two types of resonance: one due to the parallel features and the other due to the perpendicular features which show an axially symmetric anisotropy with a well-resolved 16-line hyperfine splitting characteristic of an interaction between the electron and the vanadium nuclear spin. The observed anisotropic parameter values ($g_\parallel = 1.94$, $g_\perp = 1.97$, $A_\parallel = 170$, and $A_\perp = 78$) indicate that the unpaired electron is present in the d_{xy} orbital with square-pyramidal geometry around the oxovanadium(IV) chelate [27].

The molecular orbital coefficients α^2 and β^2 were also calculated for the complex by the following equations [28]:

$$\alpha^2 = (2.0023 - g_\parallel)E/8\lambda\beta^2$$
$$\beta^2 = 7/6(-A_\parallel/p + A_\perp/p + g_\parallel - 5/14g_\parallel - 9/14g_e)$$
$$\gamma^2 = (2.0023 - g_\perp)E/2\lambda\alpha^2,$$

where $p = 128 \times 10^{-4}\,\mathrm{cm}^{-1}$, $\lambda = 135\,\mathrm{cm}^{-1}$, and E is the electronic transition energy of $^2B_2 \rightarrow {}^2E$. The lower value of $\alpha^2 = 0.77$ compared to $\beta^2 = 0.89$ indicates that the in-plane π-bonding is more covalent than the in-plane σ-bonding.

3.7. *Thermogravimetric analysis*

Thermal analysis plays an important role in the study of physicochemical behaviors and stability. All the complexes were unaffected up to ~250°C except the cobalt complex, which lost two water molecules at 150–220°C. The presence of coordinated water

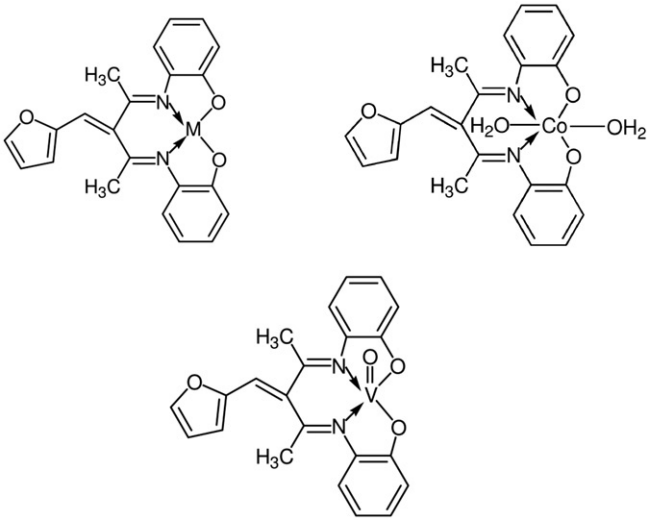

Figure 1. The structure of complexes (M = Ni(II), Cu(II), and Zn(II)).

confirms the results of analytical and IR spectra. The anhydrous complexes remained stable up to ~350°C and thereafter showed rapid degradation due to decomposition of the organic constituents of the complex molecules. The decomposition continued up to ~750°C and a stable product (as oxide) was formed as indicated by consistency in weight in the plateau of the thermogram.

Based on the above spectral data, the structures of the complexes are given in figure 1.

3.8. *DNA binding studies*

3.8.1. Electronic spectra. The absorption spectra of the copper complex in the absence and presence of CT DNA are shown in figure 2. With increasing CT DNA concentration, the hypochromism in the band at 405.5 nm reaches as high as 2.5% with a blue shift of 10 nm at a [DNA]:[complex] ratio of 10. These spectral characteristics suggest that copper complex interacts with DNA through a mode that involves a stacking interaction between the aromatic chromophore and the base pairs of DNA. After intercalating the base pairs of DNA, the π^* orbital of the intercalated ligand can couple with the π orbital of the base pairs, thus decreasing the π–π^* transition energy and resulting in the bathochromism. The coupling π orbital is partially filled by electrons, thus decreasing the transition probabilities and concomitantly resulting in hypochromism. To quantitatively compare the affinity of the synthesized complexes toward DNA, the intrinsic binding constants K_b of the synthesized complexes to CT DNA were determined by monitoring the changes of absorbance at 405.5 nm (for copper complex), 398.6 nm (for zinc complex), 395.0 nm (for cobalt complex), and 397.3 nm (for nickel complex) with the increasing concentration of DNA. The intrinsic binding constant K_b is obtained from the ratio of slope to the intercept of plots [DNA]/($\varepsilon_a - \varepsilon_f$) *versus* [DNA]. The K_b values are shown in table 1.

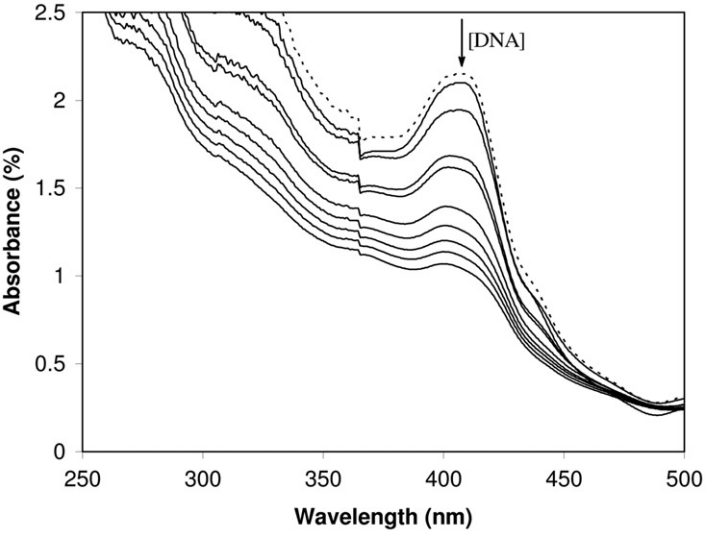

Figure 2. Electronic absorption spectrum of [CuL] in the absence (dotted line) and presence (solid line) of increasing amounts of DNA.

Table 1. Absorption spectral properties of synthesized complexes with CT DNA.

Complexes	λ_{max} Free	λ_{max} Bound	Δλ (nm)	Hypochromism (%)	$K_b \times 10^4$ ($L\,mol^{-1}$)
[CuL]	405.5	395.5	10.0	12.5	2.5
[ZnL]	398.6	392.5	6.1	4.1	1.4
$[CoL(H_2O)_2]$	395.0	391.6	3.4	2.8	1.6
[NiL]	397.3	392.0	5.3	3.9	1.9
[VOL]	389.0	388.7	0.3	−1.5	–

Comparing the intrinsic binding constant of the synthesized complexes with those of the DNA-intercalators, it is deduced that all the synthesized complexes except vanadyl complex bind strongly to DNA by intercalation. From table 1, only very weak hypochromism (−1.5%) and no significant spectral shifts are found after vanadyl complex is mixed with DNA, indicating that the vanadyl complex forms weaker adduct to CT DNA than the other complexes due to the square-pyramidal geometry of the vanadyl complex.

3.8.2. Electrochemical studies. Cyclic and DPV measurement techniques are extremely useful in probing the nature and mode of DNA binding of metal complexes. Typical cyclic voltammogram of copper complex in the absence and in the presence of varying amount of [DNA] is shown in figure 3.

In the absence of CT DNA, only one redox couple cathodic peak appears at −0.286 V for Cu(II) → Cu(I) ($E_{pa} = 0.040$ V, $E_{pc} = -0.286$ V, $\Delta E_p = 0.326$ V, and $E_{1/2} = 0.123$ V). This redox couple ratio I_{pc}/I_{pa} is approximately unity indicating that the reaction on the

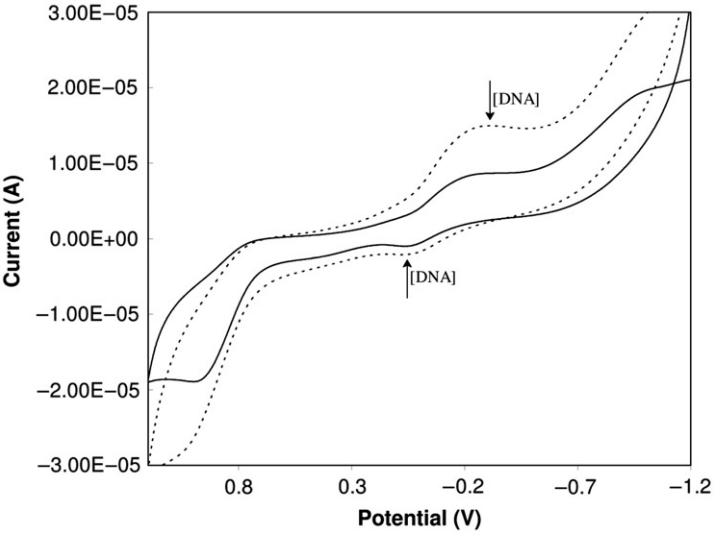

Figure 3. Cyclic voltammogram of [CuL] in the absence (dotted line) and presence (solid line) of DNA.

Table 2. Electrochemical parameters for the interaction of DNA with Co(II), Ni(II), and Cu(II) complexes.

		$E_{1/2}$ (V)		ΔE_p (V)			
Complexes	Redox couple	Free	Bound	Free	Bound	K[red]/K[oxd]	I_{pc}/I_{pa}
$[CoL(H_2O)_2]$	Co(III)/Co(II)	−0.482	−0.468	0.099	0.028	1.23	0.82
[NiL]	Ni(II)/Ni(I)	−0.342	−0.332	0.315	0.275	0.79	0.91
[CuL]	Cu(II)/Cu(I)	−0.123	−0.097	0.326	0.263	0.65	0.89

GC electrode surface is quasi-reversible. The incremental addition of CT DNA to the complex causes a negative shift in $E_{1/2}$ and a decrease in ΔE_p (table 2). The I_{pc}/I_{pa} values also decrease in the presence of DNA due to the decrease in the apparent diffusion coefficient of the copper(II) complex upon complexation with DNA. These results show that copper(II) complex stabilizes the duplex (GC pairs) by intercalation.

In the absence of CT DNA, the redox couple cathodic peak appears at 0.282 V for Co(III) → Co(II) ($E_{pa} = 0.681$ V, $E_{pc} = 0.282$ V, $\Delta E_p = 0.099$ V, and $E_{1/2} = 0.482$ V) and a second redox couple cathodic peak appears at −0.082 V for Co(II) → Co(I) ($E_{pa} = 0.299$ V, $E_{pc} = -0.082$ V, $\Delta E_p = 0.381$ V, and $E_{1/2} = 0.481$ V). The ratio I_{pc}/I_{pa} is less than unity indicating a quasi-reversible redox process. The incremental addition of CT DNA to the complex causes a negative shift in $E_{1/2}$ of 14 mV and a decrease in ΔE_p of 71 mV for the first redox couple. The I_{pc}/I_{pa} values also decrease in the presence of DNA. The decrease of the anodic and cathodic peak currents of the complex in the presence of DNA is due to decrease in the apparent diffusion coefficient of the cobalt(III) complex upon complexation with the DNA. The second redox couple of cobalt(II) complex shows no significant change of potential or intensity of current. This indicates that the second redox species does not stabilize the duplex DNA.

In the absence of CT DNA, the redox couple cathodic peak appears at −0.500 V for Ni(II) → Ni(I) ($E_{pa} = -0.185$ V, $E_{pc} = -0.500$ V, $\Delta E_p = 0.315$ V, and $E_{1/2} = 0.342$ V) and a second redox couple cathodic peak appears at −0.926 V for Ni(I) → Ni(0) ($E_{pa} = -0.643$ V, $E_{pc} = -0.926$ V, $\Delta E_p = 0.283$ V, and $E_{1/2} = 0.785$ V). The ratio I_{pc}/I_{pa} is less than unity. Incremental addition of DNA on Ni(II) complex shows a decrease in the current intensity and positive shift of the potential on the redox couple Ni(II) → Ni(I) and no significant change in the current intensity and potential on the redox couple of Ni(I) → Ni(0). The resulting changes in the current and potential demonstrate the interaction between Ni(II) and DNA.

In the absence of CT DNA, the redox couple anodic peak appears at +1.253 V with the addition of DNA to Zn(II) complex showing a decrease in the current intensity and negative shift of the oxidation peak potential. The changes in the current and potential demonstrate the interaction between Zn(II) and DNA. The electrochemical parameters of the Co(II), Ni(II), and Cu(II) complexes are shown in table 2.

DPVs of the Cu(II), Co(II), and Ni(II) complexes show a positive potential shift along with a significant decrease of current intensity. The shift in potential is related to the ratio of binding constants

$$E_b^{o\prime} - E_f^{o\prime} = 0.0591 \log\left(\frac{K[\text{red}]}{K[\text{oxd}]}\right),$$

where $E_b^{o\prime}$ and $E_f^{o\prime}$ are formal potentials of the Co(III)/Co(II) or Ni(II)/Ni(I) or Cu(II)/Cu(I) or Zn(II)/Zn(0) complex couple in the bound and free form, respectively. The ratio of the binding constants ($K_{[red]}/K_{[oxd]}$) for DNA binding of synthesized complexes were calculated and found to be less than unity. The above electrochemical experimental results indicate the preferential stabilization of Co(II), Ni(II), Cu(II), and Zn(II) forms over the other forms on binding to DNA.

DPV of the Zn(II) complex shows a negative potential shift along with significant decreasing of current intensity during the addition of increasing amounts of DNA consistent with zinc ion stabilizing the duplex (GC pairs) by intercalation. Hence, for the complex of the electroactive species (Zn(II)) with DNA, the electrochemical reduction reaction can be divided into two steps:

$$Zn^{2+} - DNA \rightleftharpoons Zn^{2+} + DNA$$
$$Zn^{2+} + 2e^- \rightleftharpoons Zn^0$$

The dissociation constant (K_d) of the Zn(II)–DNA complex was obtained using the following equation:

$$I_p^2 = \frac{K_d}{[\text{DNA}]}\left(I_p^2 o - I_p^2\right) + I_p^2 o - [\text{DNA}],$$

where K_d is the dissociation constant of Zn(II)−DNA, and $I_p^2 o$ and I_p^2 the reduction current of Zn(II) in the absence and presence of DNA, respectively. Using the above equation, the dissociation constant was determined. The low dissociation constant (2.6×10^{-10} mol L^{-1}) for Zn(II) was indispensable for the catalytic function and the structural stability of zinc enzymes which participate in replication, degradation, and translation of genetic material of all species. Zn(II) ions were probably interacting not only with the active site of the enzyme during these processes, as already well known in the literature [25], but also with DNA.

3.8.3. Viscosity measurements. Interactions between complexes and DNA were investigated by viscosity measurements. Optical photophysical probes provided necessary, but not sufficient clues to support a binding model. Hydrodynamic measurements sensitive to length change (i.e., viscosity and sedimentation) are regarded as the least ambiguous and the most critical tests of binding mode in solution in the absence of crystallographic structural data [29]. A classical intercalation model usually results in lengthening the DNA helix, as base pairs were separated to accommodate the binding ligand leading to the increase of DNA viscosity. The viscosity of CT DNA increases with the increase in the ratio of Co(II), Cu(II), and Zn(II) complexes to CT DNA. The absence of viscosity in vanadyl complex indicates that it may bind to DNA only by electrostatic force.

3.9. *DNA cleavage studies*

Gel electrophoresis using pUC19 DNA was performed with the ligand and its complexes in the presence and absence of MPA as reductant. At micromolar concentrations, for 2 h incubation period, the ligand exhibits no significant activity in the presence of MPA. The nuclease activity is greatly enhanced by the incorporation of metal ion in the ligand. The complexes cleave DNA more efficiently in the presence of reductant, which may be attributed to the formation of hydroxyl free radical. The production of a hydroxyl free radical due to the reaction between the metal complexes and oxidant may be explained as shown below:

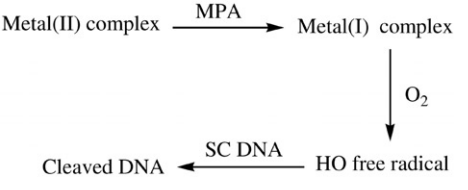

The $HO^{\bullet}$ participates in the oxidation of deoxyribose moiety, followed by hydrolytic cleavage of the sugar phosphate backbone [30]. The more pronounced nuclease activity of these adducts in the presence of reductant is due to the increased production of hydroxyl radicals. Vanadyl complex does not cleave DNA in the presence of MPA, suggesting that it binds with DNA through electrostatic mode which is further supported by the weak hypochromism in electronic absorption spectrum and no change in the viscosity effect with DNA.

3.10. *Antimicrobial activity*

The ligand and its complexes were tested for their *in vitro* antimicrobial activity against Gram-positive bacteria *S. aureus* and *B. subtilis* and Gram-negative bacteria *E. coli* and *S. typhi* by the disk diffusion method, using agar nutrient as the medium and against fungi *A. niger*, *A. flavus*, *C. albicans*, and *R. bataicola* by disk diffusion method using potato dextrose agar as medium. The MIC values of the compounds against the growth of microorganisms are summarized in tables 3 and 4.

The metal complexes exhibit higher antimicrobial activity than the free ligand [31, 32].

Table 3. Antibacterial activity of compounds.

Compound	MIC ($mg\,mL^{-1}$)			
	S. aureus	*B. subtilis*	*E. coli*	*S. typhi*
L	49	44	51	61
[CuL]	23	19	17	24
[NiL]	31	23	20	21
[ZnL]	21	15	13	18
[VOL]	28	19	18	20
$[CoL(H_2O)_2]$	24	17	16	19
Streptomycin	18	12	10	14

Table 4. Antifungal activity of compounds.

Compound	MIC ($mg\,mL^{-1}$)			
	A. niger	*A. flavus*	*C. albicans*	*R. bataicola*
L	52	63	69	59
[CuL]	12	10	13	14
[NiL]	16	18	19	21
[ZnL]	13	12	15	16
[VOL]	14	13	14	17
$[CoL(H_2O)_2]$	19	15	17	24
Nystatin	10	8	12	11

4. Conclusions

The ligand and its complexes have been characterized by microanalytical data, IR, UV-Vis, ^{1}H-NMR, ESR, and mass spectra. The complexes have composition [ML] for Cu(II), Ni(II), VO(IV), and Zn(II), but $[CoL(H_2O)_2]$ for Co(II). Intercalative binding of the Co(II), Cu(II), and Zn(II) complexes with DNA has been supported by electronic absorption spectra, cyclic voltammetry, differential pulse voltammetry, and viscometric studies. The electrostatic binding mode of vanadyl complex with DNA is observed from weak hypochromism and no significant spectral shift in electronic absorption spectrum. It is further confirmed by the absence of effect on the viscosity of DNA. The synthesized complexes except vanadyl complex exhibit nuclease activity in the presence of hydroxyl radicals. The results from *in vitro* antifungal and antibacterial tests showed that all the complexes are more active than the ligand.

Acknowledgments

The authors gratefully acknowledge the financial support of this work by the Department of Science and Technology, New Delhi, India. They express their heartfelt thanks to the VHNSN College Managing Board for providing the research facilities.

References

[1] S. Chan, W.T. Wong. *Coord. Chem. Rev.*, **138**, 219 (1995).
[2] E.-J. Gao, Q. Wu, C.-S. Wang, M.-C. Zu, L. Wang, H.-Y. Liu, Y. Huang, Y.-G. Sun. *J. Coord. Chem.*, **62**, 3425 (2009).
[3] F. Liang, P. Wong, X. Zhou, T. Li, Z.Y. Li, H.K. Lin, D.Z. Gao, C.Y. Zheng, C.T. Wu. *Bioorg. Med. Chem. Lett.*, **14**, 1901 (2004).
[4] C.N. Sudhamani, H.S. Bhojya Naik, T.R. Ravikumar, M.C. Prabhakara. *Spectrochim. Acta*, **72A**, 643 (2009).
[5] J. Sun, S.-Y. Deng, J. He, L. Jiang, Z.-W. Mao, L.-N. Ji. *J. Coord. Chem.*, **62**, 3284 (2009).
[6] L.N. Ji, X.H. Zon, J.G. Liu. *J. Coord. Chem. Rev.*, **216**, 513 (2001).
[7] N. Raman, A. Sakthivel, R. Jeyamurugan. *J. Coord. Chem.*, **69**, 3425 (2009).
[8] Q.L. Zhang, J.H. Liu, J.Z. Liu, P.X. Zhang, X.Z. Ren, Y. Liu, Y. Huang, L.N. Ji. *J. Inorg. Biochem.*, **98**, 1405 (2004).
[9] S. Murali, C.V. Sastri, B.G. Maiya. *Proc. Indian Acad. Sci. (Chem. Sci.)*, **114**, 403 (2002).
[10] D.D. Perrin, W.L.F. Armarego, D.R. Perrin. *Purification of Laboratory Chemicals*, 2nd Edn, Pergamon Press, Oxford (1980).
[11] J. Marmur. *J. Mol. Biol.*, **3**, 208 (1961).
[12] M.E. Reichmann, S.A. Rice, C.A. Thomas, P. Doty. *J. Am. Chem. Soc.*, **76**, 3047 (1954).
[13] M. Yamamata, Y. Watanabe, T. Mitsudo, Y. Nakagami. *Bull. Chem. Soc., Jpn.*, **51**, 835 (1978).
[14] D.S. Sigman, A. Spassky, S. Rimsky, H. Buc. *Biopolymers*, **24**, 183 (1985).
[15] J.B. Charies, N. Dattagupta, D.M. Crothers. *Biochemistry*, **21**, 3933 (1982).
[16] S. Satyanarayana, J.C. Daborusak, J.B. Charies. *Biochemistry*, **32**, 2573 (1983).
[17] M.J. Pelzer, E.C.S. Chan, N.R. Krieg. *Antibiotics and Other Chemotherapeutic Agents in Mirobiology*, 5th Edn, Blackwell Science, New York (1998).
[18] A. Ei-Dissouky. *Spectrochim. Acta*, **43A**, 1182 (1987).
[19] K. Nakamoto. *Infrared and Raman Spectra of Inorganic and Coordination Compounds*, 3rd Edn, Wiley Interscience, New York (1977).
[20] N. Raman, S.J. Raja, A. Sakthivel. *J. Coord. Chem.*, **62**, 691 (2009).
[21] A.B.P. Lever. *Inorganic Electronic Spectroscopy*, 2nd Edn, Elsevier, New York (1968).
[22] N. Nishat, S. Asma, S. Dhyani. *J. Coord. Chem.*, **62**, 3003 (2009).
[23] N. Raman, R. Jeyamurugan. *J. Coord. Chem.*, **62**, 2375 (2009).
[24] R.K. Ray, G.M. Kauffman. *Inorg. Chim. Acta*, **173**, 207 (1990).
[25] B.J. Hathaway, A.A.G. Tomlinson. *Coord. Chem. Rev.*, **5**, 1 (1970).
[26] K. Jayasubramanian, S.A. Samath, S. Thambidurai, R. Murugesan, S.K. Ramalingam. *Transition Met. Chem.*, **20**, 76 (1995).
[27] S.S. Dodwad, R.S. Dharmnaskar, P.S. Prabhu. *Polyhedron*, **8**, 1748 (1989).
[28] L.J. Boucher, T.F. Yen. *Inorg. Chem.*, **8**, 689 (1968).
[29] B.C. Baguley, M. Lebret. *Biochemistry*, **23**, 937 (1984).
[30] P. Merfley, E.R. Robinson. *Mutat. Res.*, **86**, 155 (1981).
[31] Y. Anjaneyalu, R.P. Rao. *Synth. React. Inorg. Met.-Org. Chem.*, **16**, 257 (1986).
[32] L. Mishra, V.H. Singh. *Indian J. Chem.*, **32A**, 446 (1993).